Electronic Supplementary Material (ESI) for Physical Chemistry Chemical Physics.

An improved spectrophotometric method tests the Einstein-Smoluchowski equation: a revisit and update

Jiangbo (Tim) Zhao[†], Cong Qi[†], Guangrui Li[†], and Markus A. Schmidt[†,‡,⊥]*

[†] Leibniz Institute of Photonic Technology, Albert-Einstein-Straße 9, 07745 Jena, Germany

[‡] Abbe Center of Photonic and Faculty of Physics, Friedrich-Schiller-University Jena, Max-Wien-Platz 1, Jena 07743, Germany

[⊥] Otto Schott Institute of Material Research, Fraunhoferstr. 6, 07743 Jena, Germany

E-mail: jiangbo.zhao@leibniz-ipht.de

Table S1. List of spectrophotometric measurements of H_2O at room temperature in the near UV to NIR wavelengths range, a complement to the summary over the period 1891-1997 in Ref. [1].

Year	Method	Instrumental	Differential path length (cm)	Mean % diff. [a]	Refs.
1934	Single-beam	Customer-designed photographic photometer	272	~ 61 [b]	[2]
1963	Single-beam	Customer-designed spectrophotometer	132	~ 17 [c]	[3]
1986	Single-beam	Customer-designed spectrophotometer	50.3	~ -55 [d]	[4]
1999	Single-beam	Customer-designed spectrophotometer	150	~ 2.1 [e]	[1]
2009	Double-beam	Commercial spectrophotometer	0.9	~ 9900	[5]
2012	Single-beam	Customer-designed spectrophotometer	100	~ 105 [f]	[6]
2015	Double-beam	NA	5	~ 181	[7]
2017	Single-beam	Customer-designed ellipsometer	20	~ 323	[8]
2019	Double-beam	Commercial spectrophotometer	0.5	~ -22	This work

[a] Mean % diff. = 100% $(Exp_1-Exp_2)/Exp_2$, where $Exp_{1,2}$ represent the extinction coefficients from the reference as noted, and from the publication by Segelstein [9], respectively. Unless specified, the extinction coefficient refers to the figure at 480 nm.

[b,c] Mean % diff. calculations refer to the extinction coefficients at 400 nm since the figures at 480 nm are absent.

[d] Mean % diff. calculation refers to the extinction coefficient at 436 nm due to the absence of data at 480 nm.

[e] Mean % diff. calculation refers to the extinction coefficient at 400 nm because of negative value at 480 nm.

[f] Mean % diff. calculation refers to the extinction coefficient at 500 nm, the starting wavelength of the measurement.

Table S2. Parameters used for calculation of scattering coefficients of solvents H_2O, D_2O, DMSO, and DMSO-d_6. Unless specified, the tabulated data exemplify the figures for H_2O at 344 nm, for D_2O at 650 nm, and for DMSO and DMSO-d_6 both at 500 nm. Empirical scattering coefficient $\tilde{b}$ for H_2O and measured extinction coefficients $\tilde{\mu}$ for the other three solvents, are shown in the table, respectively.

	Δ	β_T (×10^{-10})	γ (×10^{-10})	n [f]	$\tilde{b}$ or $\tilde{\mu}$ (×10^{-4})	$\tilde{b}$ (×10^{-4})	% diff. [g]
		m²/N	mN/m		dB/cm (Exp)	dB/cm (Eq.7&8)	
H_2O	0.108 [a]	4.58 [10]	71.98 [11]	1.35008	7.71	5.93	30
D_2O	0.111 [b]	4.74 [12]	71.87 [13]	1.33243	4.30	0.43	900
DMSO	0.436 [c]	5.32 [10]	43.54 [14]	1.48194	317.8	8.70	3553
DMSO-d_6	0.439 [d]	5.28 [e]	43.7 [15]	1.47801	197.6	8.41	2250

[a] The depolarization ratio Δ for H_2O is the mean of the measured values in the reference. [16]

[b] The net difference of depolarization ratio Δ between D_2O and H_2O is 0.003, thus yielding 0.111 for D_2O. [17]

[c] The depolarization ratio Δ for DMSO is given by extrapolating the solvent's Δ in the temperatures range 30-48 °C to the room temperature via a polynomial fit (R^2=1). [18] The extrapolated value 0.436 for DMSO is valid, considering 0.453 for the structurally similar solvent Dimethylformamide (DMF). [19]

[d] The depolarization ratio Δ for DMSO-d_6 is about 0.439, obtained by assuming that the net difference in [b] is retained for the pair of solvents DMSO and DMSO-d_6.

[e] The isothermal compressibility β_T for DMSO-d_6, not found in the literature, is derived on the basis of equation $\beta_T \gamma^{7/4} = \text{constant}$, [20] where γ is the surface tension, and "constant" for solvent DMSO is lent to DMSO-d_6 because the products $\beta_T \gamma^{7/4}$ between H_2O and D_2O are nearly equal.

[f] Listing of refractive indices n at 25 °C for the wavelengths as specified in the table caption for the respective solvents. The full data set of refractive indices for different solvents across the wavelengths concerned refer to an index-related Manuscript in preparation by Zhao J, *et al*., for the sake of consistency (factors like material, temperature, etc.) though many other literature have reported the index values.

[g] % diff. = (Exp-Cal)/Cal, where Exp is the measured coefficient, and Cal represents the calculated results.

Section S1. Experimental preparations and instrumental evaluation

Accurate measure of extinction coefficients for chemically pure and optically transparent solvent is not as simple and straightforward as it looks. For the sake of reproducibility and rigor in research, we enumerate in detail all of the procedures pertinent to the spectrophotometric measurement.

S1.1 Solvent

Ultrapure H_2O, with resistivity of 18.2 MΩ-cm and total organic carbon (TOC) below 1 ppb, is supplied by a SG Ultra Clear UV plus TM/EI-Ion® system. Deuterated water (D_2O, 99.9 atom % D), dimethyl sulfoxide (DMSO for spectroscopy, purity ≥ 99.8 %) and deuterated DMSO (DMSO-d_6, 99.9 atom % D) are purchased from Sigma-Aldrich and used without further purification. The solvents are only dispensed before the measurement conduct.

In general, a high-purity solvent, particularly ultrapure H_2O, is the corrosive substance, which leaches away present impurities from the parts that the solvent comes into contact with. To minimise this contaminating possibility, we thoroughly cleaned containers such as Pyrex glass vial, PTFE/silicone septum and cuvette, before their use.

S1.2 Cuvette

The use of quality and flawless cuvette is entailed, because in addition to being as a sample container, cuvette is automatically a part of the optical system once placed in the compartment. In this work we purchase brand-new Hellma 110-QS Quartz Glass cuvettes (high performance, 200-2500 nm), with 0.5 and 1.0 cm path lengths (tolerance accuracy ± 0.001 cm). We only qualify the cuvette for the experiment if the one in empty can maintain transmissions above 80 % from 200-2500 nm throughout a complete pre-check (that is the repeated spectrophotometric measurements of the cuvette of interest with its frequent in- and out-placement in the compartment). To avoid the post-incurred defects during the experiment, we handle the cuvettes with great care, including transfer, placement, cleaning, etc.

S1.3 Cleaning

The cleaning procedure is carried out as follows: immersing the parts, such as cuvettes, glass vials and PTFE lids, in ~ 2% (v/v) Hellmanex III cleaner solution for about 30 min, followed by ultrasonication for less than 5 min at moderate temperature (to facilitate the cleaning), before rinse in sequence by flowing ethanol, distilled H_2O, and ultrapure H_2O, and then purging N_2 for drying. Note that, to effectively leach away residual impurities, we apply ultrapure H_2O for rinsing lastly; and to minimise the physical adsorption of airborne contaminants and particulates, we either clean the parts right before the use or store them in desiccator immediately after cleaning.

S1.4 Spectrophotometer

For the best measurement performance across the wavelengths 350-1400 nm, we use double-beam Spectrophotometers JASCO V-660 (working wavelength 187-900 nm) and V-670 (working wavelength 190-2700 nm) for different spectral regions (see detailed discussions below).

To ensure the thermal equilibrium, we warm up the sspectrophotometers for more than 60 mins. To acquire stable baseline characteristic, good signal-to-noise ratio and spectra shape, we set the parameters as: spectra resolution 0.5 nm, scanning speed 100 nm/min, and medium response, with the bandwidths 2 nm for the wavelengths range < 900 nm and 8 nm for that > 900 nm. We chose the change wavelength 900 nm for the grating and detector in V-670.

S1.5 Instrumental capacity – baseline flatness and baseline drift

Strictly speaking, the beams' photon flux densities in the reference and sample compartments in double-beam spectrophotometer are disparate, corresponding to unequal photocurrents upon the detector. To eliminate this disparity, it is the usual practice to conduct the baseline correction scan, through which the null current between the beams is accounted, and in that time and in that environment, the "zero absorbance" for the instrument is recognised. Ideally with the baseline correction scan, the subsequent spectrophotometric scans should allow to directly and accurately measure the absorbance of the sample. But the instrument imperfection renders the baseline never unchanged over the time and across the wavelengths. In other words, the baseline characteristics, such as baseline flatness (also called instrumental noise) and baseline drift (a.k.a. absorbance stability), would influence the spectrophotometer's capacities, like the accuracy, precision and detection limit of the instrument.

Baseline flatness (instrumental noise)

The baseline flatness levels of the two spectrophotometers are specified by the manufacturer, both ± 0.0005 Abs over the wavelengths 200-800 nm. Given that switching of light sources, gratings and detectors could take places over an extended wavelengths range from 350-1400 nm, we reckon that the instrumental noise across the wavelengths of interest likely differ from what the manufacturer has claimed. We thus undertake re-evaluation of the baseline flatness for both spectrophotometers, by means of conduct of six individual "zero absorbance"

measurements. Note that, in an attempt to remove interference by baseline drift (as discussed in the subsequent subsection), we perform the baseline correction scan before conducing every "zero absorbance" measurement, i.e., six baseline correction scans in total.

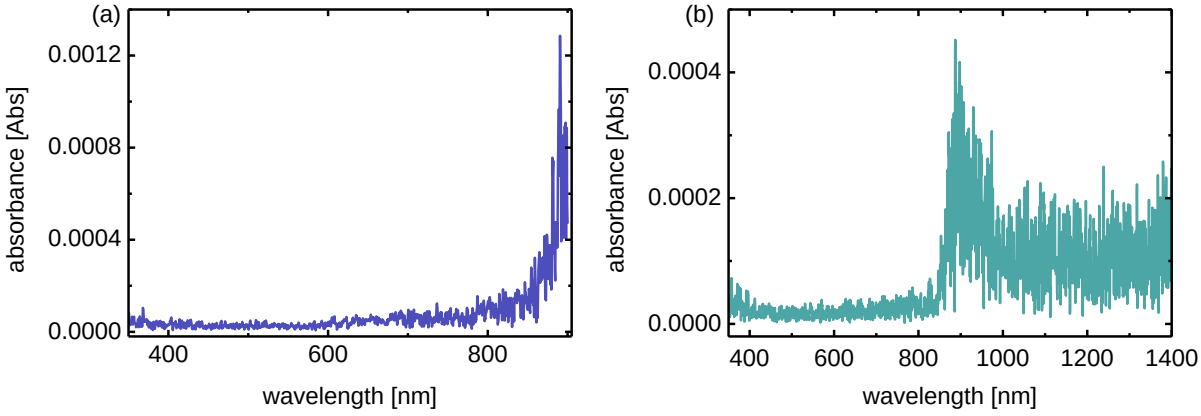

Fig. S1 The respective instrumental noises of Spectrophotometers V-660 (a) and V-670 (b), obtained by applying the standard deviation (SD) equation to the six "zero absorbance" scans (for a reduced sampling bias).

As shown in Fig. S1a, the instrumental noise of V-660 is within ± 0.00003 Abs from 350-650 nm, multiplies in between ± 0.00005 Abs for the range 650-800 nm, and mounts up to ± 0.001 Abs for 800-900 nm, reflecting the suffering sensitivity of photomultiplier tube (PMT) as the wavelength increases. In Fig. S1b, it shows the instrumental noise of V-670 stabilises within ± 0.00003 Abs from 350-850 nm, ascends to ± 0.0004 Abs from 850-950 nm (due of the switching of detectors, e.g., from PMT to PbS photoconductive cell, and associated filters), and then falls to ± 0.0002 Abs in the wavelengths range 950-1400 nm. These results indicate that, with regard to the baseline flatness, spectrophotometers V-660 and V-670 are interchangeable.

Baseline drift (absorbance stability)

Along with filter switching, light source exchanging, etc., each additional scan would drift the baseline. After multiple scans, the drift cumulates in a way that the instrument's on-going baseline could much differ from the initially recorded baseline. Paradoxically, the resulting absorbance is accounted for by the initial baseline record instead of the real-time baseline. This suggests that the baseline drift should incur the deviation of measured values from actual absorbance, and the drift' degree determines the accuracy level of the measurement. For measurement involving multiple scans over a period of time, evaluation of baseline drift is essential and necessary.

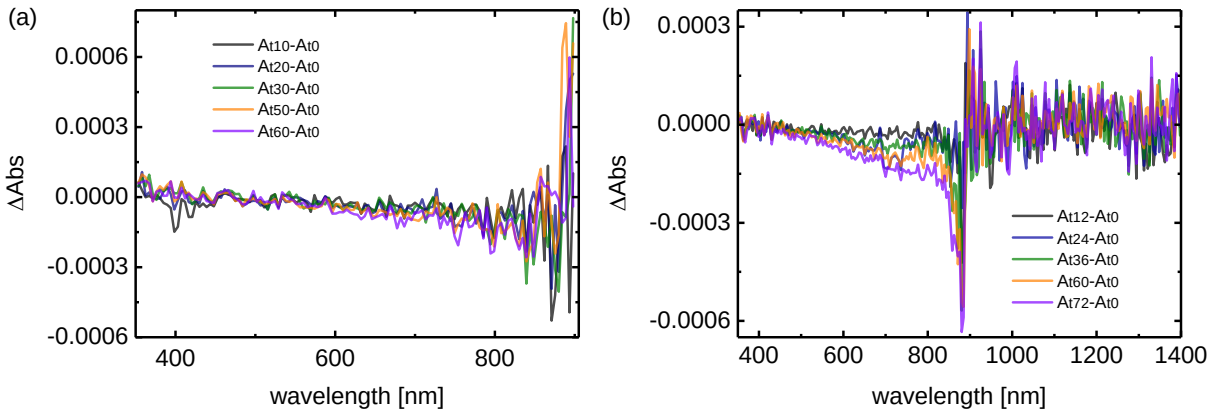

Fig. S2 Characterisations of baseline drift for Spectrophotometers V-660 (a) and V-670 (b). $|A_{t1} - A_{t2}| = \Delta Abs$, where $A_{t1/2}$ represent the absorbance measured at time t_1 and t_2 relative to the baseline scan t=0, and ΔAbs is the net difference in the time intervals as defined. Different from the baseline flatness evaluation where baseline correction scan is needed to be undertaken for every "zero absorbance" measurement, the characterisation of baseline drift only performs baseline correction scan once.

As shown in Fig. S2a, the baseline drift for spectrophotometer V-660 is inconsiderable over the wavelengths 350-900 nm in 60 minutes, i.e., $|A_{t0} - A_{t10}| = |A_{t0} - A_{t60}|$. For spectrophotometer V-670, its baseline drift is negligible from 850-1400 nm, while raising

progressively in the wavelengths range 350-850 nm, e.g., from less than 0.00001 Abs in 12 min to 0.00005~0.0004 Abs in 72 min (Fig. S2b). To access the best accuracy that we could, we decide to use spectrophotometers V-660 and V-670, for 350-850 nm and 850-1400 nm, respectively.

With scanning speed at 100 nm/min, the time of every scan for V-660 (from 350-850 nm) and V-670 (from 850-1400 nm) are about 5 and 5.5 min, respectively. This means that, for the Four-step method measurement, each spectrophotometer spends about 22 min in measuring (for four scans), and as suggested in Fig. S2, the baseline drifts are both negligible over this duration.

Defining signal-to-noise ratio (SNR) 2:1 as threshold (2σ), and taking into account baseline flatness and baseline drift, we confirm that the combined use of spectrophotometers offers the detection limit at 0.00006 Abs from 350-850 nm, around 0.0008 Abs from 850-950 nm, and less than 0.0004 Abs from 950-1400 nm.

Section S2. Spectrophotometric measurement

S2.1 Beer-Lambert law

According to the Beer-Lambert law, the absorbance (*A*, namely extinction) and transmittance (T_t) for a medium are depicted as:

$$A = -Log_{10}\left(\frac{I_t}{I_0}\right) = -Log_{10}T_t = \mu L \qquad \text{(S1)}$$

where I_0 and I_t are the radiant fluxes of the incident and transmitted light, μ is the decadic extinction coefficient of the medium (unit: cm^{-1}), and L is the path length. The decadic extinction coefficient μ in unit of cm^{-1} can be converted to the extinction coefficient $\tilde{\mu}$ in unit of dB/cm, via the relation $\tilde{\mu} = 10\mu$. If needed, the napierian extinction coefficient in literature

is converted into decadic form by multiplying a factor of $1/Ln10$. In this work, we use $\tilde{\mu}$ (or μ) as a measure for the solvent's extinction per unit length.

The extinction coefficient (μ or $\tilde{\mu}$) is the sum of the absorption coefficient (a or $\tilde{a}$) and scattering coefficient (b or $\tilde{b}$), which is described as:

$$\mu = a + b \text{ or } \tilde{\mu} = \tilde{a} + \tilde{b}. \qquad \text{(S2)}$$

S2.2 Optical paths in cuvettes

The way a ray of incident light traverses the empty and liquid-filled cuvettes is distinct. Appreciation of their differences in optical paths between the cuvettes is a prerequisite for advancing the spectrophotometric method.

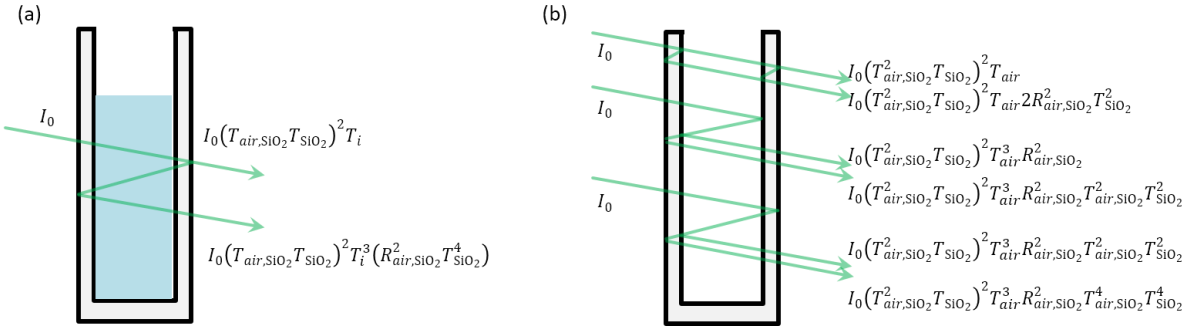

Fig. S3 Schematic diagrams of the optical paths in the liquid-filled (a) and empty (b) cuvettes. The schematics illustrate the total transmitted light containing the fluxes that have undergone multiple reflections, refractions, and transmissions at the interfaces and over the mediums. For visualization, the normal incidence is sketched intentionally with angle. Given that the thickness of glass wall and the path length of cuvette involved in this work are larger than 0.1 cm (and the spectral bandwidth > 2 nm), the possible light interference effect is neglected. [5]

Liquid-filled cuvette

As exemplified in Fig. S3a, the total transmitted light $I_{t,f}$ passing through the liquid-filled cuvette is constituted as:

$$I_{t,f} = I_0\left(T_{air,\mathrm{SiO_2}}T_{\mathrm{SiO_2}}\right)^2 T_i\left(\underbrace{1}_{once\ medium\ trasverse}\right.$$

$$+ \underbrace{R^2_{air,\mathrm{SiO_2}}T^4_{\mathrm{SiO_2}}T^2_i}_{thrice\ medium\ trasverses} \qquad \text{(S3)}$$

$$\left. + \underbrace{R^4_{air,\mathrm{SiO_2}}T^8_{\mathrm{SiO_2}}T^4_i}_{five\ times\ medium\ trasverses} + \cdots\right)$$

where $R_{i,\mathrm{SiO_2}}$ and $T_{i,\mathrm{SiO_2}}$ are the reflection and transmission for an interface between the medium (either the air or a specific solvent) and cuvette, and $T_{\mathrm{SiO_2}}$ and T_i are the transmissions for the cuvette glass wall and for the medium in cuvette, respectively. The reflections and transmissions, for an interface, are described by Fresnel equations $R_{i,\mathrm{SiO_2}} = \left(\frac{n_{\mathrm{SiO_2}} - n_i}{n_{\mathrm{SiO_2}} + n_i}\right)^2$ and $T_{i,\mathrm{SiO_2}} = 1 - R_{i,\mathrm{SiO_2}}$, where $n_{\mathrm{SiO_2}}$ and n_i are the refractive indices of the cuvette and medium, respectively. The transmissions of the quartz glass and medium are described as $T_{\mathrm{SiO_2}} = 10^{-\mu_{\mathrm{SiO_2}}L_{\mathrm{SiO_2}}}$ and $T_i = 10^{-\mu_i L_i}$, where $\mu_{\mathrm{SiO_2}}(\text{and } \mu_i)$ and $L_{\mathrm{SiO_2}}(\text{and } L_i)$ are the extinction coefficients and path lengths.

In the wavelength range concerned, $R_{air,\mathrm{SiO_2}}$ is less than 0.037, T_{air} for air and $T_{\mathrm{SiO_2}}$ for glass walls both approximately equal to 1, and T_i always less than 1, hence the sum of the geometric series in eqn (S3) becomes:

$$I_{t,f} = I_0\left(T_{air,\mathrm{SiO_2}}T_{\mathrm{SiO_2}}\right)^2 T_i(1 + \delta_f) \qquad \text{(S4)}$$

where δ_f, the ratio of a total amount of the higher-order transmitted light to the first-order counterpart, is in the approximation to $0.001T_i^2$. This is the eqn (1) in the main text.

Empty cuvette

As shown in Fig. S3b, the higher-order transmitted light for an empty cuvette consists of the light that passes through the medium once, thrice, and so on, and air-glass interface for six, eight times, etc. Including the first-order transmitted light, the total transmitted light is summed as:

$$I_{t,e} = I_0\left(T_{air,\mathrm{SiO_2}}^2 T_{\mathrm{SiO_2}}\right)^2 T_{air}\Big(\underbrace{1 + 2R_{air,\mathrm{SiO_2}}^2 T_{\mathrm{SiO_2}}^2}_{once\ medium\ trasverse} + \underbrace{R_{air,\mathrm{SiO_2}}^2 T_{air}^2 + 2R_{air,\mathrm{SiO_2}}^2 T_{air,\mathrm{SiO_2}}^2 T_{\mathrm{SiO_2}}^2 T_{air}^2 + R_{air,\mathrm{SiO_2}}^2 T_{air,\mathrm{SiO_2}}^4 T_{\mathrm{SiO_2}}^4 T_{air}^2}_{thrice\ medium\ trasverses} + \cdots\Big). \quad \text{(S5)}$$

The summed amount of this infinite series is further simplified to:

$$I_{t,e} = I_0\left(T_{air,\mathrm{SiO_2}}^2 T_{\mathrm{SiO_2}}\right)^2 T_{air}(1 + \delta_e), \quad \text{(S6)}$$

where δ_e, the ratio of a total amount of the higher-order transmitted light to the first-order counterpart, lies within 0.0063~0.0078. This is the eqn (2) in the main text.

Albeit higher-order transmissions, such as $I_0\left(T_{air,\mathrm{SiO_2}} T_{\mathrm{SiO_2}}\right)^2 T_i \delta_f$ and $I_0\left(T_{air,\mathrm{SiO_2}}^2 T_{\mathrm{SiO_2}}\right)^2 T_{air}\delta_e$, in minor quantity, the direct omissions of these terms from eqn (S4) and (S6) are not recommended, as their presences are helpful to stress the criterion that a pair of cuvettes used during the measurement must be as much clean, quality, and identical as possible.

Section S3. Four-step method

S3.1 Experimental operations

As named, the Four-step method includes four spectrophotometric scans for two-different-length cuvettes in the sample compartment. The operation is specified as follows in order: making the baseline correction scan → performing the spectrophotometric scan for short-length cuvette in empty (Step 1) → filling the liquid of interest in the cuvette followed by running another spectrophotometric scan (Step 2) → replacing with a long-length empty cuvette and then conducting the scan (Step 3) → undertaking the last scan for the liquid-filled long-length cuvette (Step 4). Importantly, to minimise the experimental uncertainties, any inserted cuvettes are kept immobile without touching until the cuvette replacement.

S3.2 Theoretical derivation

The incident light I_0, dispensed from a stable lamp source under a DC power, is supposed to be invariant. The selected cuvettes after pre-check are viewed as nearly equal, i.e., $n_{\mathrm{SiO_2}}$ and $T_{\mathrm{SiO_2}}$ are almost the same between the cuvettes. As long as these conditions are simultaneously met (so that unknown terms linked to the cuvettes are eliminable), the substitution of the incident light I_0 and the transmitted light $I_{L1,e,s}$, $I_{L1,f,s}$, $I_{L2,e,s}$, and $I_{L2,f,s}$ in eqn (S4) and (S6) into eqn (S1) gives:

$$\begin{aligned}\Delta A_{L1,s} &= A_{L1,f,s} - A_{L1,e,s} \\ &= -Log_{10}\left(\frac{T_{L1,f,s}}{T_{air,\mathrm{SiO_2}}^2 T_{air}}\frac{1+\delta_{L1,f,s}}{1+\delta_{L1,e,s}}\right)\end{aligned} \tag{S7}$$

and

$$\begin{aligned}\Delta A_{L2,s} &= A_{L2,f,s} - A_{L2,e,s} \\ &= -Log_{10}\left(\frac{T_{L2,f,s}}{T_{air,\mathrm{SiO_2}}^2 T_{air}}\frac{1+\delta_{L2,f,s}}{1+\delta_{L2,e,s}}\right).\end{aligned} \tag{S8}$$

Subtraction between eqn (S8) and (S7) derives μ, as:

$$\mu = \frac{\Delta A_{L2,s} - \Delta A_{L1,s}}{L_2 - L_1} + \frac{Y}{L_2 - L_1} \quad \text{(S9)}$$

and Y is described as:

$$Y = Log_{10}\left(\frac{1 + \delta_{L2,f,s}}{1 + \delta_{L1,f,s}}\frac{1 + \delta_{L1,e,s}}{1 + \delta_{L2,e,s}}\right) = Log_{10}\left(\frac{1 + \delta_{L2,f,s}}{1 + \delta_{L1,f,s}}\right). \quad \text{(S10)}$$

Eqn (S9-S10), i.e., eqn (3-4) in the main text, are the mathematical expression of the Four-step method. The term Y describes the contribution from the higher-order transmitted light, where, for different-length cuvettes (assumed identical), the glass walls hold the equality between $\delta_{L1,e,s}$ and $\delta_{L2,e,s}$, but the different lengths lead to the disparity between $\delta_{L2,f,s}$ and $\delta_{L1,f,s}$, as indicated in eqn (S3) and (S5). Given the solvent's extinction coefficients from 0.00001 to 0.1 cm^{-1} (L_1=0.5 cm and L_2=1.0 cm), the term $Y/(L_2 - L_1)$ varies between -2.0·10^{-8} and -1.4·10^{-4} cm^{-1}, corresponding to errors from -0.20 % to -0.14 %. This Y is inconsiderable and neglected during the execution of eqn (S9), but its retention in the formula is used to emphasize the criterion that the cuvettes must be as identical as possible.

S3.3 Theoretical derivation of the Two-step method

Similar to the derivation process for the Four-step method, formulation of the "Two-step method" for solvent extinct coefficient is written as:

$$\mu = \frac{A_f - A_e}{L_{2,s} - L_{1,r}} + 2Log_{10}\left(\frac{T_{air,\mathrm{SiO_2},L2,s}}{T_{air,\mathrm{SiO_2},L1,r}}\right) + \frac{Y}{L_{2,s} - L_{1,r}}, \quad \text{(S11)}$$

where $A_f = Log_{10}\frac{I_{t,f,L1,r}}{I_{t,f,L2,s}}$, $A_e = Log_{10}\frac{I_{t,e,L1,r}}{I_{t,e,L2,s}}$, and Y is described as:

$$Y = Log_{10}\left(\frac{1 + \delta_{L1,f,r}}{1 + \delta_{L2,f,s}}\frac{1 + \delta_{L2,e,s}}{1 + \delta_{L1,e,r}}\right). \quad \text{(S12)}$$

The beams between the sample (*s*) and reference (*r*) channels are different, hence the second and third items in eqn (S11) cannot be eliminated. Any cuvettes are imperfect, such that the differences between the two items are further amplified. This accounts for the large errors when using the Two-step method, because omission of the last two items in eqn (S11), as a majority of measurements exercised to date, makes the extinction coefficient measured largely deviate from the true value.

Section S4. Compilation of measurement uncertainties

S4.1 Theoretical compilation of measurement uncertainties

For the Four-step method, extraction of solvent extinction coefficient relies on eqn (S9). A propagation of error of the variables in eqn (S9) yields the extinction coefficient uncertainty, expressed as:

$$S_{\mu}^{2} = \left(\frac{1}{L2-L1}\right)^{2} S_{(\Delta A_{L2,s}-\Delta A_{L1,s})}^{2} + \frac{\left(\Delta A_{L2,s}-\Delta A_{L1,s}\right)^{2}}{(L2-L1)^{4}} S_{(L2-L1)}^{2} - 2\frac{\Delta A_{L2,s}-\Delta A_{L1,s}}{(L2-L1)^{3}} S_{AL}^{2}, \quad \text{(S13)}$$

where

$$S_{(\Delta A_{L2,s}-\Delta A_{L1,s})}^{2} = S_{A_{L2,f,s}}^{2} + S_{A_{L2,e,s}}^{2} + S_{A_{L1,f,s}}^{2} + S_{A_{L1,e,s}}^{2} \quad \text{(S14)}$$

$$S_{(L2-L1)}^{2} = S_{L2}^{2} + S_{L1}^{2}. \quad \text{(S15)}$$

The cross term S_{AL} is not given since its sum approaches zero.

The standard deviation of the absorbance, S_A, is described as:

$$S_A^2 = \left(\frac{\partial A}{\partial L}\right)^2 S_L^2 + \left(\frac{\partial A}{\partial \theta}\right)^2 S_\theta^2 + \left(\frac{\partial A}{\partial n_{SiO_2}}\right)^2 S_{n_{SiO_2}}^2, \quad \text{(S16)}$$

where S_L, S_θ and $S_{n_{SiO2}}$ are the standard deviations for the corresponding variables, and possible covariances between θ, L and n are negligible, and

$$\frac{\partial A}{\partial L} = \mu \quad \text{(S17)}$$

$$\frac{\partial A}{\partial n_{SiO_2}} = \left(\frac{1}{n_{SiO_2}} - \frac{1}{n_{SiO_2}+1} - \frac{1}{n_{SiO_2}+n_i}\right)\frac{4}{\ln 10}. \quad \text{(S18)}$$

The full expression $\frac{\partial A}{\partial \theta}$ is a function of $sin\,\theta$, thus $\lim_{\theta \to 0} \frac{\partial A}{\partial \theta} = 0$, suggesting the error from the small uncertainty of θ is not consequential. Substitution of eqn (S14-S18) into eqn (S13) yields the SD for extinction coefficient as:

$$S_\mu = \frac{1}{L2-L1}\sqrt{6\mu^2 S_L^2 + \frac{64}{(\ln 10)^2}\left(\frac{1}{n_{SiO_2}} - \frac{1}{n_{SiO_2}+1} - \frac{1}{n_{SiO_2}+n_i}\right)^2 S_n^2}. \quad \text{(S19)}$$

The variables concerned here are not intended to be exhaustive. For example the insignificant temperature fluctuation is not considered. As suggested by Højerslev and Trabjerg [21] and Röttgers *et al.*, [22] the temperature-dependent offset is at the level of 10^{-7} cm^{-1} $°C^{-1}$, which is ignorable against the aforesaid variables' uncertainties.

S4.2 Experimental validation of the measurement limit

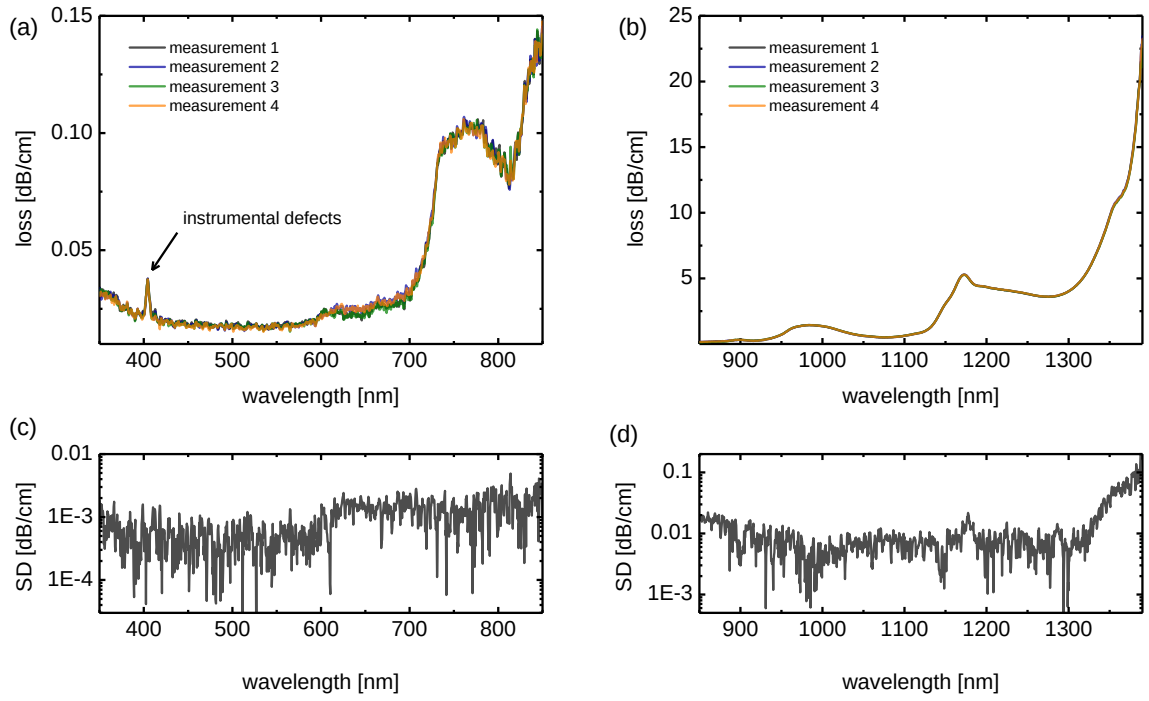

Fig. S4 The Four-step method-measured extinctions in H_2O-DMSO mixture (with mass ratio 70:30), over (a) 350-850 nm for V-660, (b) and 850-1400 nm for V-670 (×4 measurements, equivalent to a total of ×16 scans for each spectrophotometer). (c, d) The SD of extinction coefficients in the mean of ×16 scans for the corresponding spectrophotometers, in good agreement with the detection limit discussed in Section S1.5.

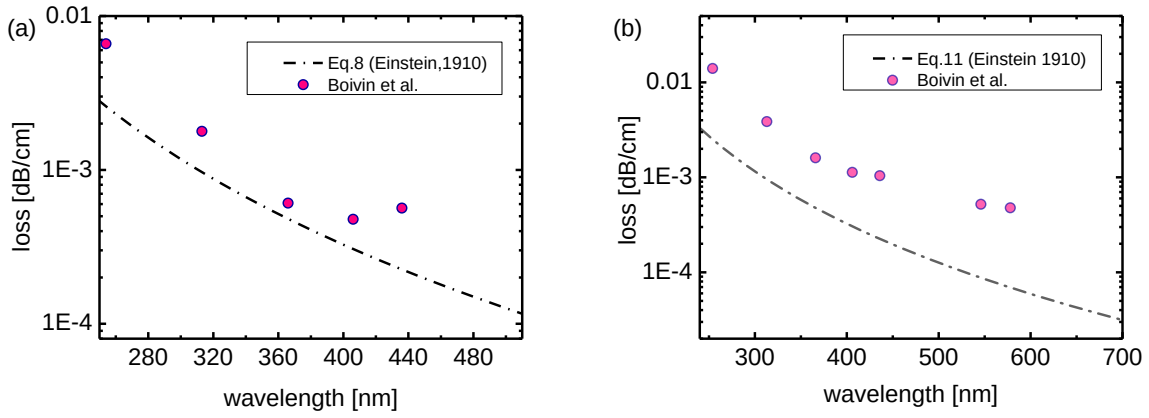

Fig. S5 The extinction coefficients for solvents (a) H_2O and (b) D_2O, where the record-low extinctions (filled circles) measured by the One-step method, [4] are overlaid with the theoretical predications according to the Einstein-Smoluchowski equation (dash-dot lines).

Section S5. Summary of fundamental vibration frequencies in solvents

Solvent H_2O exhibits three fundamental vibrations associated with two OH bonds, including symmetric (υ_1) and asymmetric (υ_3) stretch, and bending (υ_2), with resonances maxima of approximately 3277 cm^{-1} (3.05 μm), 3490 cm^{-1} (2.87 μm) and 1645 cm^{-1} (6.08 μm). Solvent H_2O's absorptions around 606, 739 and 970 nm are assigned to the respective *n*th harmonics of stretching, and 1200 nm resonance peak indexed to the combination band of 2nd overtone of stretching and fundamental bending. [23-26]

For DMSO, in addition to the weak rocking vibrations of CH_3 at 1019 and 1031 cm^{-1}, the solvent gives rise to multiple prominent broad resonances, such as the fundamental stretching vibrations from CH_3, CH_2, & CH in range of 2850-3000 cm^{-1} (3.33-3.50 μm), the fundamental bending resonances from CH_2&CH_3-deformations between 1350-1470 cm^{-1} (6.8-7.4 μm), the SO fundamental stretching modes from 1041-1052 cm^{-1} (9.5-9.6 μm), and the CSC fundamental stretching vibrations from 667-697 cm^{-1} (14.3-15.0 μm). DMSO's characteristic bands with maxima at 627, 736, 901 and 1180 nm and a span of 680-740, 756-822, 850-925, 971-1057, 1133-1233 and 1360-1400 nm arise from the overtones of $CH_{1,2,3}$-stretching vibrations (2-9th overtones) and CH_2&CH_3-deformations (4-9th overtones), respectively. [27-31]

References

1 Litjens, R. A., Quickenden, T. I. & Freeman, C. G. Visible and near-ultraviolet absorption spectrum of liquid water. *Applied optics* **38**, 1216-1223 (1999).

2 Dawson, L. & Hulburt, E. The absorption of ultraviolet and visible light by water. *JOSA* **24**, 175-177 (1934).

3 Sullivan, S. A. Experimental study of the absorption in distilled water, artificial sea water, and heavy water in the visible region of the spectrum. *JOSA* **53**, 962-968 (1963).

4 Boivin, L.-P., Davidson, W., Storey, R., Sinclair, D. & Earle, E. Determination of the attenuation coefficients of visible and ultraviolet radiation in heavy water. *Applied optics* **25**, 877-882 (1986).

5 Otanicar, T. P., Phelan, P. E. & Golden, J. S. Optical properties of liquids for direct absorption solar thermal energy systems. *Solar Energy* **83**, 969-977 (2009).

6 Kedenburg, S., Vieweg, M., Gissibl, T. & Giessen, H. Linear refractive index and absorption measurements of nonlinear optical liquids in the visible and near-infrared spectral region. *Optical Materials Express* **2**, 1588-1611 (2012).
7 Li, X., Liu, L., Zhao, J. & Tan, J. Optical properties of sodium chloride solution within the spectral range from 300 to 2500 nm at room temperature. *Applied spectroscopy* **69**, 635-640 (2015).
8 Wang, C., Tan, J. & Liu, L. Wavelength and concentration-dependent optical constants of NaCl, KCl, MgCl 2, CaCl 2, and Na 2 SO 4 multi-component mixed-salt solutions. *Applied optics* **56**, 7662-7671 (2017).
9 Segelstein, D. J. *The complex refractive index of water*, University of Missouri--Kansas City, (1981).
10 Bachmann, S. J. & van Gunsteren, W. F. Polarizable model for DMSO and DMSO–water mixtures. *The Journal of Physical Chemistry B* **118**, 10175-10186 (2014).
11 Petrova, T. & Dooley, R. Revised release on surface tension of ordinary water substance. *Proceedings of the International Association for the Properties of Water and Steam, Moscow, Russia*, 23-27 (2014).
12 Reisler, E. & Eisenberg, H. Refractive Indices and Piezo-optic Coefficients of Deuterium Oxide, Methanol, and Other Pure Liquids. *The Journal of Chemical Physics* **43**, 3875-3880 (1965).
13 Cooper, J. & Dooley, R. IAPWS release on surface tension of heavy water substance. *International Association for the Properties of Water and Steam (IAPWS), Charlotte, NC* (1994).
14 Schrader, A. M. *et al.* Correlating steric hydration forces with water dynamics through surface force and diffusion NMR measurements in a lipid–DMSO–H2O system. *Proceedings of the National Academy of Sciences* **112**, 10708-10713 (2015).
15 http://www.chemspider.com/Chemical-Structure.67699.html.
16 Kratohvil, J., Kerker, M. & Oppenheimer, L. Light scattering by pure water. *The Journal of Chemical Physics* **43**, 914-921 (1965).
17 Cohen, G. & Eisenberg, H. Light scattering of water, deuterium oxide, and other pure liquids. *The Journal of Chemical Physics* **43**, 3881-3887 (1965).
18 Haynes, L. L., Schmidt, R. L. & Clever, H. L. Thermodynamic properties of acetone, dimethyl sulfoxide, and their solutions by Rayleigh light scattering. *Journal of Chemical and Engineering Data* **15**, 534-536 (1970).
19 Katime, I., Cesteros, L. C. & Strazielle, C. Light scattering from binary mixtures of 1, 2-dichloroethane, acetonitrile, dimethylformamide and ethyl acetate. Excess gibbs functions. *Journal of the Chemical Society, Faraday Transactions 2: Molecular and Chemical Physics* **80**, 1215-1224 (1984).
20 McGowan, J. The isothermal compressibilities of liquids. *Recueil des Travaux Chimiques des Pays-Bas* **76**, 155-164 (1957).
21 Trabjerg, I. & Højerslev, N. K. Temperature influence on light absorption by fresh water and seawater in the visible and near-infrared spectrum. *Applied optics* **35**, 2653-2658 (1996).
22 Röttgers, R., McKee, D. & Utschig, C. Temperature and salinity correction coefficients for light absorption by water in the visible to infrared spectral region. *Optics express* **22**, 25093-25108 (2014).
23 http://www1.lsbu.ac.uk/water/water_vibrational_spectrum.html.
24 Mason, J. D., Cone, M. T. & Fry, E. S. Ultraviolet (250–550 nm) absorption spectrum of pure water. *Applied optics* **55**, 7163-7172 (2016).
25 Pope, R. M. & Fry, E. S. Absorption spectrum (380–700 nm) of pure water. II. Integrating cavity measurements. *Applied optics* **36**, 8710-8723 (1997).
26 Tam, A. & Patel, C. Optical absorptions of light and heavy water by laser optoacoustic spectroscopy. *Applied Optics* **18**, 3348-3358 (1979).

27 Groh, W. Overtone absorption in macromolecules for polymer optical fibers. *Die Makromolekulare Chemie: Macromolecular Chemistry and Physics* **189**, 2861-2874 (1988).

28 https://www2.chemistry.msu.edu/faculty/reusch/VirtTxtJml/Spectrpy/InfraRed/infrared.htm.

29 Wallace, V. M., Dhumal, N. R., Zehentbauer, F. M., Kim, H. J. & Kiefer, J. Revisiting the aqueous solutions of dimethyl sulfoxide by spectroscopy in the mid-and near-infrared: experiments and Car–Parrinello simulations. *The Journal of Physical Chemistry B* **119**, 14780-14789 (2015).

30 Oh, K. I., Rajesh, K., Stanton, J. F. & Baiz, C. R. Quantifying Hydrogen-Bond Populations in Dimethyl Sulfoxide/Water Mixtures. *Angewandte Chemie* **129**, 11533-11537 (2017).

31 Plidschun, M., Chemnitz, M. & Schmidt, M. A. Low-loss deuterated organic solvents for visible and near-infrared photonics. *Optical Materials Express* **7**, 1122-1130 (2017).